Development of a high backdrivable partially powered Swing assistive actuator knee design: a multiobjective optimization framework

Development of a high backdrivable partially powered Swing assistive actuator knee design: a multiobjective optimization framework

Andrea Berettoni[1,2], Simone Traverso[2], Samuele De Giuseppe[2,3], Carlo De Benedictis[2], Carlo Ferraresi[2], Nicolò Boccardo[1,3] and Matteo Laffranchi[1]

***Abstract*—This manuscript presents a multiobjective optimization framework for high backdrivable partially powered swing assistive actuator knee design. The research exploits a Serial Elastic Actuator (SEA), in parallel with a motor valves controlled hydraulic cylinder, with the purpose of expanding the prosthesis capabilities into the power quadrants of the power plane, without sacrificing the benefits relative to existing microprocessor-controlled-knee prostheses (MPKs), able to allow a strictly-passive ballistic swing-phase. The mechatronic design parameters are optimized by exploiting the multi-objective evolutionary genetic algorithm and validated by means of a knee prosthesis multibody model. The backdrive torque found with the described model corresponds to a relatively low value of 2.56 Nm at the knee joint, allowing the pursued high backdrivability of the system.**

***Index Terms*—Transfemoral, prosthesis, partially powered, biomechanics, amputation, backdrivability.**

I. Introduction

In the United States alone, approximately 600,000 individuals cope with major lower limb amputations, half of whom have transfemoral amputations (TFAs) [1], [2], a prevalence projected to rise more than double by 2050 and magnified globally, ranging from 20-30 times higher [3]. Many activities of daily living (ADL) are trickier for transfemoral amputees compared to their aged-matched amputee counterparts [4], [5]. TFAs, in particular, significantly impact mobility, as patients often experience reduced walking speed, heightened susceptibility to joint injuries, an increased risk of falls and an asymmetric gait pattern [6]–[9].

The majority of prosthetic devices are designed with a focus on walking on flat terrain, prioritizing the provision of stability during weight-bearing phases and ensuring proper knee movement during the swinging phase of walking. In particular, given that in healthy subjects walking typically demands negative energy expenditure, the swinging motion on level ground arises from inertial interaction between the shank and thigh, characterized by low-resistance behaviour at the knee. This phenomenon, termed ballistic motion, entails the knee being predominantly influenced by the hip movement, establishing inertial coupling with the prosthetic device [10], [11].

The most common type of commercially available knee prosthesis is a microprocessor-controlled knee (MPK), which incorporates stance control via modulated dampers that actively vary the amount of damping from high impedance needed for knee stability to a much lower impedance necessary to guarantee the cited ballistic swing-phase motion. Although these types of prostheses allow for versatile gait patterns and stability with the capability to adapt to different walking speeds, downward slopes, and other activities based on energy dissipation such as stair descent and sitting down, they still lack an actuation unit that can exert positive work to assist in energetically positive activities such as sit-to-stand and stair climbing. In fact, activities with slower movement compared to walking (e.g. stair ascending) or movement in which the ballistic inertial coupling is not achieved (e.g. sit-to-stand activity) lead to the impossibility of reaching a desired knee motion through hip movement. Typically, prosthetic users adopt either a step-to or a step-over technique. In the context of microprocessor-controlled knees (MPKs), both methods involve minimal or no knee movement during the swing phase, with the affected limb essentially being dragged along. However, individuals frequently resort to compensatory actions to negotiate obstacles, such as hip circumduction, ankle vaulting, or pelvic tilting, particularly when using energetically passive prostheses [12].

In comparison to MPKs, powered prostheses exist that are capable of providing the full spectrum of the power plane (i.e., both active and braking torque-speed behaviours). However, achieving such functionality necessitates a large motor and transmission ratio, potentially leading to elevated output impedance and audible noise, thereby posing challenges to device acceptance. Furthermore, recent human-centred design approaches highlight how users prioritize reliability, comfort, low weight and cost compared to versatility [13]. Consequently, ongoing research endeavours concentrate on integrating advantageous features from both passive and active technologies into partially powered prostheses, aiming to alle-

This research was supported by the Istituto Nazionale per l'Assicurazione contro gli Infortuni sul Lavoro (INAIL) under grant agreement PR19-PAI-P1 – HyperLEG.

[1]A. Berettoni, S. Traverso, S. De Giuseppe, N. Boccardo and M. Laffranchi are with the Rehab Technologies IIT-INAIL Lab, Italian Institute of Technology, Via Morego 30, 16163, Genova, Italy.

[2]A. Berettoni, C. De Benedictis and C. Ferraresi are with the Department of Mechanical and Aerospace Engineering, Polytechnic University of Turin, Turin, 10129 Italy.

[3]S. De Giuseppe, N. Boccardo are with The Open University Affiliated Research Centre at Istituto Italiano di Tecnologia (ARC@IIT) which is part of the Open University, Milton Keynes MK7 6AA, United Kingdom.

viate the limitations associated with fully powered counterparts while acknowledging certain constraints in device versatility. To address this design challenge, recent investigations have delved into methodologies such as disengaging the actuation unit from the joint or targeting specific subsets of active tasks (i.e. partially powered). This approach yields prosthetic devices that are more compact and lighter and emit reduced acoustic noise in comparison to fully active alternatives that might lead to device abandonment [14].

In this context, the authors present a layout for the actuation unit of a partially powered knee prosthesis based on a hydraulic damper and a Series Elastic Actuator (SEA), aimed at addressing both high-speed and high-torque demands of several motion tasks. A scheme of this layout is shown in Fig. 1. The proposed architecture should keep the desired features of passive systems, yet allowing to inject mechanical power when needed. Following the exposition of the rationale for the requirements and the subsequent selection of actuation method, the authors employ a multiobjective analysis to achieve an optimal transmission ratio. Subsequently, utilizing multibody simulations, a backdrivability analysis has been performed to assess the actuator's capacity to facilitate a strictly passive biomimetic swing-phase motion and estimate the actuator's power consumption.

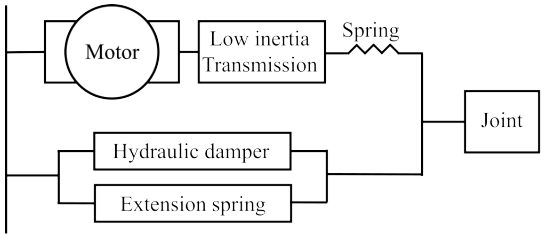

Fig. 1: Proposed actuation block diagram

II. Requirements

In recent years, there has been a growing interest among researchers in utilizing high-torque motors coupled with low-ratio transmissions (i.e. Quasi Direct-Drive actuator (QDD)). This motor-transmission configuration offers several advantages, including reduced impact from unmodeled dynamics, enhanced robustness, and closer approximation to an ideal model, which facilitates the implementation of simplified control strategies [15], [16]. However, a notable challenge arises from the physical dimensions of high-torque motors, particularly when they are positioned at the knee axis of rotation. Placing the motor in this configuration notably widens the space between the knee axis of rotation and the top of the pyramid connection. This change in position affects the shape of the prosthesis, potentially diminishing its psychological acceptance due to a departure from anthropometric standards [17]. Considering this distance as $26\,\mathrm{mm}$ in a widely used MPK prosthesis, such as the C-Leg Prosthesis [18], we have imposed a constraint to limit the outer diameter at $50\,\mathrm{mm}$.

Looking at the different ambulation activities, walking is usually not very demanding since it mostly involves negative joint powers at the knee joint [19]. Level walking predominates in daily occurrences, thus commanding primary attention in design considerations. Although tasks involving ascending stairs and sit-to-stands are relevant, their frequency significantly trails behind that of level walking. However, when it comes to going up stairs, a slow speed and increased torque of over $1\,\mathrm{N\cdot m/kg}$ is required which may lead to a heavy and bulky actuator. However, related to this design the resistive torque is fully provided by the hydraulic cylinder capable of providing more than $0.55\,\mathrm{N\cdot m\cdot s/(rad\cdot kg)}$ and a dissipative power of $3.5\,\mathrm{W/kg}$ (i.e. more than 50th male percentile).

During the swing phase of walking on level ground, knee motion is largely driven by hip motion, resulting in a ballistic movement. As a result, knee motion can be achieved without active power at the joint. Therefore, to realize a natural ballistic movement, the prosthetic knee has to feature a low impedance, by featuring low rotational inertia, damping and friction [20]. Based on prior work, to ensure swing-phase dynamics remain unaffected by actuators and drivetrains, it is preferable to limit the reflected inertia of these components at less than 10% of the rotational inertia of the biological shank and foot around the knee joint, approximately $380\,\mathrm{kg\cdot cm^2}$ [21].

Based on data from healthy individuals, biological knee provides a damping constant of approximately $1\,\mathrm{N\cdot m\cdot s/rad}$ [22], and a minimum damping constant of $0.5\,\mathrm{N\cdot m\cdot s/rad}$ [23]. To achieve our goal of designing a compliant partially powered knee prosthesis with a lower resistive torque compared to the biological knee joint, the choice was to consider a velocity of about $3.3\,\mathrm{rad/s}$ since it is the velocity used to investigate the backdrivability analysis in the following sections. Consequently, the resistive torque of the biological knee joint is calculated by the product of the damping and the selected speed, which is $3.3\,\mathrm{N\cdot m}$.

In case of tasks featured with non-ballistic knee movement such as swing during stair ascent, powered assistance has been shown perturbation robustness in cases of disturbances (e.g. stumble) [24]. Since the minimum active torque will be computed from the following model, only the active knee angle trajectory tracking might be identified by at least $3.5\,\mathrm{rad/s}$. Overall, the requirements are summarized in Tab. I.

TABLE I: Actuator requirements.

Design Requirement	***Target Values***		***Unit***
	Lower Bound	Upper Bound	
Pyramid-to-knee distance		50	mm
Reflected Inertia		380	$\mathrm{kg\cdot cm^2}$
Damping coeff.		1	$\mathrm{N\cdot m\cdot s/rad}$
Resistive Torque	3.3		$\mathrm{N\cdot m}$
Active Speed	3.5		$\mathrm{rad/s}$

III. Optimization methodology

To optimize the proposed actuation scheme we develop a dynamic simulation framework widely used in wearable robotics devices (e.g. [15], [25]). The simulation framework

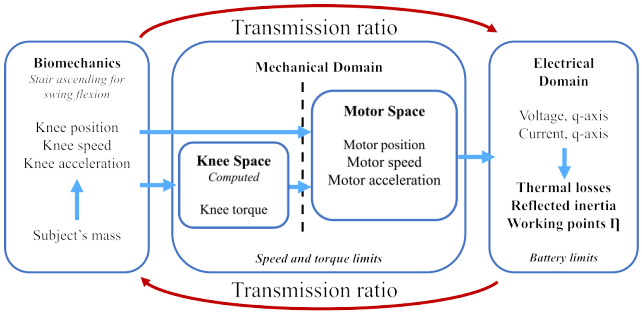

Fig. 2: Overview of the actuation optimization framework.

is based on a multi-step design process that, starting from the desired knee joint biomechanics at swing flexion (SF) stair ascending, explores all the possible configurations within a defined parameter space. For each possible configuration, the simulation framework computes the required motor torque, speed, voltage and current, while also estimating the electrical energy consumption. Fig. 2 presents the schematic of the presented optimization framework. At the core of this method, there is the development of a reliable model of the knee prosthesis actuation block. In the following, the main steps followed for the definition of the model are presented. Then, the multi-objective optimization technique and its implementation are outlined.

A. Model

1) Biomechanics: Biomechanic data that is selected as the input of the optimization concerns the swing flexion at stair ascending of the 50th American men percentile (i.e. user mass of 78.4 kg) [26], where only the kinematics data are taken into account, whereas torque profiles are computed within the model.

2) Mechanical domain: The prosthesis dynamics aims to translate the problem from joint space to motor space in function of all the components that affect the motor torque

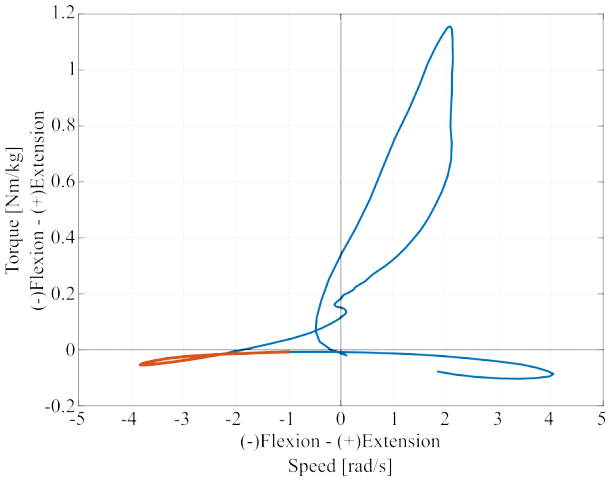

Fig. 3: Torque-speed requirements at stair ascending, in red swing flexion phase.

requirement (T_m). Fig. 4 highlights a simplified linear model representation of the knee actuation block in the mechanical domain.

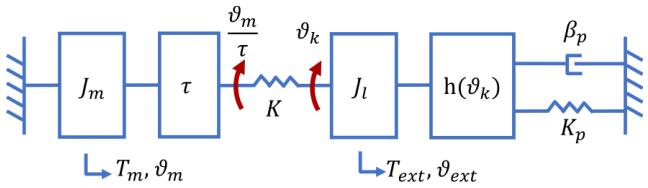

Fig. 4: Linear model representation of the hybrid knee dynamics.

System dynamics is expressed by equations (1)-(3) where only the gravity term is considered as external force (T_ext) since the analysis is performed at the swing flexion stage with no contact between foot and ground. The transmission ratio between the rotary motion of the knee joint (T, w) and the linear motion of the cylinder (F, v) is governed by the variable lever arm length $h(\theta_k)$, proportional to the knee angle as shown in equations (2). Thus, the reaction torque generated by the passive elements is related to the variable lever arm and spring deformation $s_h(\theta_k)$, which depends on the spring unit length. J_l is the combined inertia of the prosthesis shank and foot about the knee joint axis described in II, J_m is the inertia of the motor, while the angular position of the motor and the knee joint are θ_m and θ_k, respectively. In this manuscript, we focus on gear ratio τ, leaving spring design for future work to really exploit the multi-objective optimization algorithm's capabilities. Thus, a rigid configuration with infinite stiffness is considered.

$$\begin{cases} T_\mathrm{ext} + J_l \ddot{\vartheta}_\mathrm{ext} = T_a + T_p \\ \vartheta_\mathrm{ext} = \vartheta_k \\ \dot{\vartheta}_\mathrm{m} = \dot{\vartheta}_\mathrm{k} \tau \end{cases} \tag{1}$$

$$\begin{cases} T_p = (\beta_p \dot{x} + k_p \Delta x) h(\theta_k) \\ \Delta x = s_h(\theta_k) \\ \dot{x} = \dot{\vartheta}_k h(\theta_k) \end{cases} \tag{2}$$

$$\begin{cases} T_\mathrm{ext} = mgl \sin(\vartheta_k) \\ T_a = (T_m \eta - J_m \ddot{\vartheta}_\mathrm{m}) \tau \\ \eta = \eta_m \eta_{tr} \end{cases} \tag{3}$$

The model formulation requires the identification of parameters such as the damping provided by the hydraulic cylinder. Fig. 5 highlights the linear pneumatic test bench used to estimate the minimum linear damping of the retained hydraulic cylinder, that is the one obtained at fully opened hydraulic valve position. That resulted in a value of β_p equal to $1274\,\mathrm{N \cdot s/m}$.

3) Electrical domain: Given the mechanical requirements, the brushed d.c. electromechanical model was developed to define the electrical demands as shown in equations (4):

$$\begin{cases} i_\mathrm{m} = \frac{T_\mathrm{m}}{K_\mathrm{t}} \\ v_\mathrm{m} = i_\mathrm{m} R^\phi + K_\mathrm{b} \dot{\vartheta}_\mathrm{m} + L^\mathrm{q} \frac{\mathrm{d}i_\mathrm{m}}{\mathrm{d}t} \end{cases} \tag{4}$$

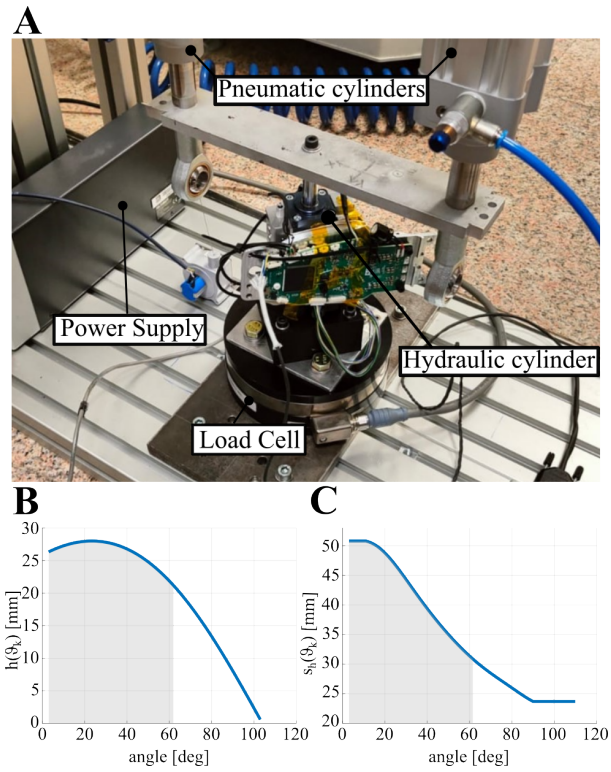

Fig. 5: A) Minimum damping characterization with a pneumatic test bench. B) Lever arm length and C) spring deformation in functions of knee angle. Grey area represents the walking range of motion.

To fulfil user needs requirements on limiting the distance between pyramid to knee axis rotations, the chosen electric machine is a TQ RoboDrive ILM50x08, 210 W servo motor. Star serial and delta serial configurations were taken into account both in simulation and experimentally. For the former, since the intention is to use q-axis current as motor current to compute the resistive heat loss, the required winding resistance is the phase resistance that might be different from the terminal resistance presented on the BLDC motor datasheets [27]. In particular, the winding type highly influenced the conversion from terminal resistance to phase resistance, thus the terminal resistance can be scaled as shown in Equation 5; same reasoning for inductance.

$$\text{Star}: \begin{cases} R^{\phi} = \frac{1}{2}R^{ll} \\ L^{q} = \frac{3}{2}L^{ll} \end{cases} \quad \text{Delta}: \begin{cases} R^{\phi} = \frac{3}{2}R^{ll} \\ L^{q} = \frac{1}{2}L^{ll} \end{cases} \tag{5}$$

Similarly to the mechanical domain, some parameters are estimated from the field to identify the model prior to the implementation of the optimization methodology. In particular, torque constant characterization and experimental efficiency map of the two motors have been obtained with a test bench, Fig. 6. The requirements of having high backdrivable system allows the choice of a star serial configuration with a higher torque constant but with no load speed of 3300 rpm that is high enough to perform fast activities such as swing at walking.

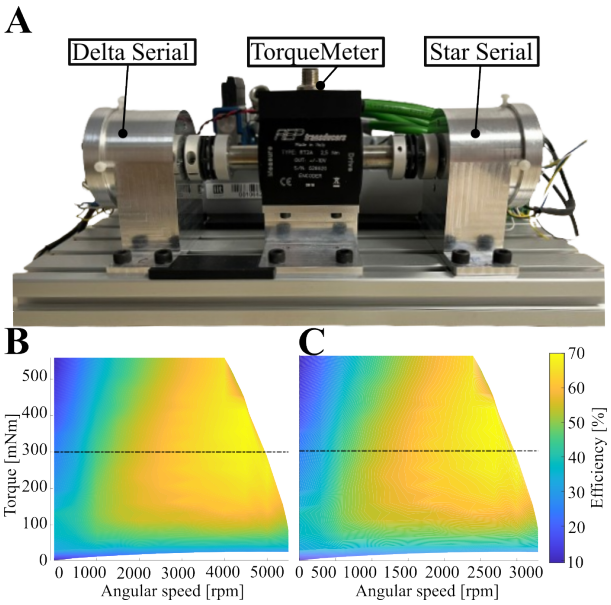

Fig. 6: A) Efficiency map test bench.(B) Delta Serial motor. (C) Star Serial motor.

B. *Multi-objective optimization problem formulation*

Multi-Objective Optimization (MOO) deals with problems where conflicting objectives require finding a set of solutions that balance multiple criteria. In MOO, the goal is to identify Pareto-optimal solutions, representing trade-offs between competing objectives [28]. Mathematically it can be written as:

$$\min_{\mathbf{X}} \{f_1(\mathbf{X}), f_2(\mathbf{X}), \ldots, f_m(\mathbf{X})\}$$

$$\begin{aligned} \text{s.t. } & g_i(\mathbf{X}) \leq 0, \quad i = 0, 1, \ldots, p \\ & h_j(\mathbf{X}) = 0, \quad j = 0, 1, \ldots, q \\ & \mathbf{X}_L \leq \mathbf{X} \leq \mathbf{X}_U \\ & \mathbf{X} = [x_1, x_2, \ldots, x_n]^T \end{aligned}$$

Considering $f_m(\mathbf{X})$ as the m-th objective function, $g_i(\mathbf{X})$ as the i-th inequality constraint, $h_j(\mathbf{X})$ as the j-th equality constraint, and $\mathbf{X}$ as the vector of design variables. Additionally, $\mathbf{X}_L$ and $\mathbf{X}_U$ represent the vectors of lower and upper bounds, respectively. These constraints define the variable space, $\mathbb{R}^n$, within which the algorithm searches for optimal solutions.

The presented optimization framework exploits the transmission ratio as a design variable where the transmission efficiency $\eta(\mathbf{tr})$ has been estimated at 90%.

The first objective function is the reflected inertia. Only the motor inertia is evaluated as the mass and shape of the transmission strongly depend on the design choice and property of the materials. The objective function is expressed as

$$f_1(\mathbf{X}) = J_{ref} = J_m \tau^2 \tag{6}$$

where J_m is the inertia coming from the motor datasheet. Thus, minimizing the reflected inertia leads to directly reducing the reduction ratio.

The second objective function concerns the power losses due to Joule heating. The other sources of losses such as bearing friction, air resistance, core losses due to hysteresis and eddy current are neglected both for the difficulty of retrieving information from manufacturer datasheet, plus Joule heating is generally the dominant factor that leads to temperature rising.

$$f_2(\mathbf{X}) = P_{loss} = i_m^2 R^{\phi} \tag{7}$$

The third objective function concerns the motor efficiency experimentally characterized as shown in Section III-A3.

$$f_3(\mathbf{X}) = \eta_m = \frac{T_m w_m}{v_m i_m} \tag{8}$$

Design constraints should be defined to bound the algorithm search space. First, the maximum current limit strictly depends on the electronic board used that imposes a maximum current of 15 A. Thus, the first constraint is formulated as

$$g_1(\mathbf{X}) = -i_m - i_{max} \leq 0 \tag{9}$$

The second constraint is related to the winding voltage limit that intrinsically limits the maximum reachable speed, the choice was at 24 V.

$$g_2(\mathbf{X}) = -v_m - v_{max} \leq 0 \tag{10}$$

The third constraint is based on the maximum efficiency of the motor physically tested that corresponds at 71 %.

$$g_3(\mathbf{X}) = -\eta_m - \eta_{max} \leq 0 \tag{11}$$

To conclude, the fourth constraint is related to the maximum reflected inertia previously defined in Section II that corresponds to $380\,\mathrm{kg}\cdot\mathrm{cm}^2$.

$$g_4(\mathbf{X}) = -J_{ref} - J_{refMax} \leq 0 \tag{12}$$

C. Optimization Results

Genetic algorithm was initialized with a population size of 200 chromosomes, with 100 as the maximum algorithm iterations and a tolerance in constraints and objective functions of 10^{-3} and 10^{-4}, respectively. The geometric constraint chosen to limit the possible transmission ratio is:

$$5 \leq \tau \leq 100 \tag{13}$$

Fig. 7 presents the Pareto front of the algorithm versus the transmission ratio design variable. By the intersection of two planes, we identify heuristically a set of optimal transmission ratios that span between 28 and 36 and correspond to reflected inertia lower than $100\,\mathrm{kg}\cdot\mathrm{cm}^2$ and a motor efficiency greater than 50%.

IV. Validation

The result of MOO leads to the identification of the theoretical optimal value for the transmission ratio. Then, the actual mechanical design of the gearbox comes into play to achieve feasible solutions that eventually fulfill that requirement. In general, the retained range of transmission ratio previously derived might be achieved with a compound gear based on the structural characteristics of the planetary gearbox.

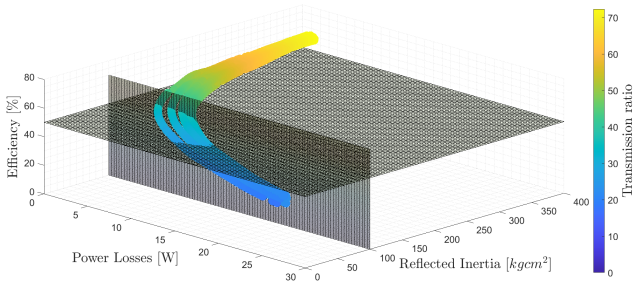

Fig. 7: Pareto front of the MOO problem. Two planes were used to identify a possible range of transmission ratios.

To validate the actuation choice, the actuation model has been developed exploiting the MATLAB Simscape environment. The choice was to use the transmission value identified in the previous section (i.e. 36:1) with two reduction stages of 6:1. The decision is based on two possible reasons. First, it is important to evaluate the worst-case scenario among the optimal conditions, as this can provide validation for lower gear ratios. On the other hand, this transmission ratio can be compared with the experimental and analytical results from Zhu *etal.* [29] that accurately estimate the backdrive torque (eq. (14)). This estimation takes into account the combined motor inertia and other rotating inertia within the transmission, as well as velocity-dependent terms derived from motor characterization in Section III-A3, eq. (15).

$$T_b = \frac{(T_{emf} + T_n)\tau + J_{tot}\ddot{\vartheta}_{\mathrm{k}}}{\eta_{tr}} \tag{14}$$

$$T_{emf} = K_{\mathrm{t}} \frac{\dot{\vartheta}_{\mathrm{m}}}{K_v R^{\phi}}, \qquad T_n = K_{\mathrm{t}} i_0 \tag{15}$$

The planetary spur gear, constructed using MISUMI stock parts with a chosen modulus of 0.5, was designed to limit the radial dimension to the outer stator diameter. Table II highlights the parameters of one planetary transmission stage.

TABLE II: Parameters of the planetary gearbox.

	Sun	Planet	Ring
Modulus		0.5	
Gear width [mm]		5	
Material		medium carbon steel	
Number of planets		3	
Number of teeth	16	32	80

The corresponding gears, with the chosen motor, were drawn and imported in a Simscape environment. To validate the overall actuator backdrivability, the prosthesis has been modelled horizontally on a benchtop to eliminate the gravity effect, fixing the knee joint-ring gear to the bench (i.e. trasmission frame), and leaving the prosthesis body-final planetary

carrier (i.e. trasmission output) free to be externally rotated. A load cell, oriented perpendicularly to the longitudinal axis of the prosthesis, has been integrated into the prosthesis body to measure the acceleration-related component of the backdrive torque model. The analysis was performed by externally imposing on the prosthesis frame a rotation of $\pm 60\,\mathrm{deg}$ at a cadence of 3 seconds.

After examining the device's passive walking capabilities, we analyzed its power consumption in different conditions. This included assessing the power consumption at the knee actuator during swing flexion while ascending stairs through simulation and the power usage by the hydraulic valve motor during walking and idle periods through experimental measurements.

V. Results

Figure 8 presents the backdrive torque as estimated by the multi-body model. This estimation revealed a similar behavior to that reported in [29] with a root-mean-square (RMS) dynamic backdrive torque of $2.56\,\mathrm{N\cdot m}$. Other than that, to increase the accuracy of the model, also the linear passive elements (T_p in Section III-A2) were incorporated, increasing the resistive torque by 15%, resulting in an RMS value of $2.94\,\mathrm{N\cdot m}$. This validates the device's ability to walk passively and suggests the potential for energy regeneration, as well as the implementation of simplified control strategies (e.g. no need for transparency control).

To explore the motor capabilities in stair ascending mode, another simulation was conducted, where the actuator was commanded with a torque reference and a desired trajectory (i.e. knee angle trajectory at swing flexion) was imposed on the knee joint. The simulation highlighted an average power consumption of $204\,\mathrm{W}$ with an average current of $8.5\,\mathrm{A}$ per stride, considering a commercial LiPo battery ($24\,\mathrm{V}$ nominal, $1.5\,\mathrm{A\cdot h}$ capacity, 129600 Joule). Additionally, during the characterization procedures, we measured the power consumption related to the off-the-shelf hydraulic valve motor (Faulhaber 1016M009SR model) powered at $9\,\mathrm{V}$ corresponding to an average power of $0.96\,\mathrm{W}$ and current $0.11\,\mathrm{A}$ per walking stride. Furthermore, we measured the overall system consumption in an idle state, with all the motors enabled but not moving. As a reference, we considered the daily occurrences of walking and stair climbing of healthy subjects [30] and a 14-hour duty cycle as the total daily power consumption. The analysis, resumed in Table III, shows that the retained knee prosthesis can operate for almost 2.5 days of usage. However, this calculation does not include other ambulation activities, like going downstairs and transitions from sitting to standing, which could affect the prosthesis's total energy usage.

TABLE III: Daily power consumption.

Activity	Walking	Stair ascent-SF	Idle state	Total
Occurrence/day	5500 steps	47-66 stairs	-	
Average Current [A]	0.11	8.5	0.07	
Average Power [W]	0.96	204	0.86	
Elapsed time [s]	1.41	0.24	-	
Energy per stride [J]	1.35	48.96	-	
Overall Energy [J]	7425	3231	49536	**60192**

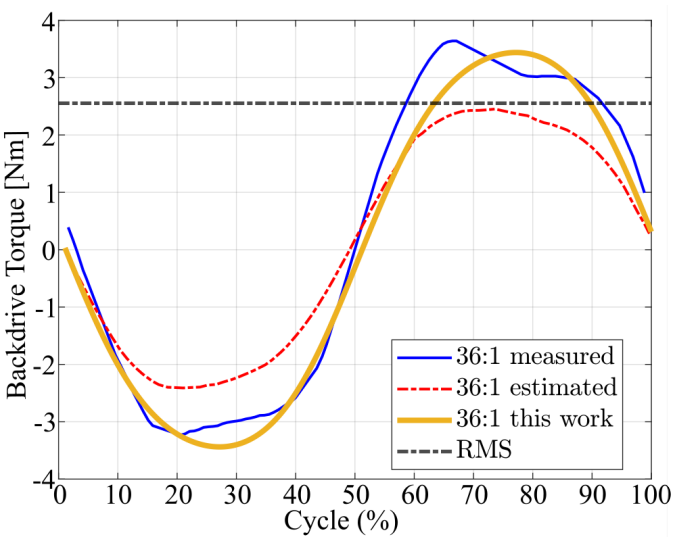

Fig. 8: Backdrive torque model compared with [29] showing a $2.56\,\mathrm{N\cdot m}$ dynamic backdrive torque.

VI. Conclusion

This study presents the development of a high backdrivable partially powered actuator knee design. The device capitalizes on the established advantages of traditional MPK prostheses while facilitating swing assistance without compromising passive quadrant behaviors in the torque-speed plane. Additionally, it enables strictly passive ballistic swing-phase motion. The proposed device incorporates a series elastic actuator at the knee joint, featuring a high torque density motor with a limited outer diameter to minimize the pyramid-to-knee-joint length. It also integrates a low-ratio, backdrivable transmission connected in parallel to a hydraulic damper equipped with flow control valve. This combination allows for the exploitation of the passive architecture during high torque braking tasks and the injection of active power when needed. In particular, other than providing the full torque range during swing, such actuator may also exploit assistance up to 17% during stance extension at stair ascending and 15% in sit-to-stands, relative to healthy subjects requirements [31]. First, this manuscript presents an optimized framework for depicting an optimal transmission ratio using an evolutionary genetic algorithm for multi-objective optimization. Then, a multibody model of the chosen actuator was implemented to validate the proposed design.

Results showed the prosthesis capability similar to a MPK prosthesis able to walk passively concurrently with the possibility to inject power on demand. Future works will focus on the experimental validation of the proposed high backdrivable partially powered actuator.

REFERENCES

[1] K. Ziegler-Graham, E. J. MacKenzie, P. L. Ephraim, T. G. Travison, and R. Brookmeyer, 'Estimating the prevalence of limb loss in the United States: 2005 to 2050', Arch Phys Med Rehabil, vol. 89, no. 3, pp. 422–429, Mar. 2008, doi: 10.1016/j.apmr.2007.11.005.

[2] M. Owings M, Kozak L. Ambulatory and inpatient procedures in the United States, 1996, Vital Health Statistics, 1998, 139, https://pubmed.ncbi.nlm.nih.gov/9866429/

[3] R. Renzi, N. Unwin, R. Jubelirer, and L. Haag, 'An International Comparison of Lower Extremity Amputation Rates', Annals of Vascular Surgery, vol. 20, no. 3, pp. 346–350, May 2006, doi: 10.1007/s10016-006-9044-9.

[4] I. C. Narang, B. P. Mathur, P. Singh, and V. S. Jape, "Functional capabilities of lower limb amputees," Prosthet. Orthot. Int., vol. 8, no. 1, pp. 43–51, 1984.

[5] C. Gauthier-Gagnon, M. C. Grisé, and D. Potvin, "Enabling factors related to prosthetic use by people with transtibial and transfemoral amputation," Archives of Physical Medicine and Rehabilitation, vol. 80, no. 6. pp. 706–713, 1999.

[6] Gauthier-Gagnon C.,Grise M. C., and Potvin D., Enabling factors related to prosthetic use by people with transtibial and transfemoral amputation, Archives of Physical Medicine and Rehabilitation, 1999, 80(6), pp. 706-13, https://doi.org/10.1016/S0003-9993(99)90177-6

[7] Talbot L. A., Musiol, R. J., Witham E. K., and Metter E. J., Falls in young, middle-aged and older community dwelling adults: perceived cause, environmental factors and injury, BMC Public Health, 2005, 5(86), https://doi.org/10.1186/1471-2458-5-86

[8] Schmalz T., Blumentritt S. and Marx B, Biomechanical analysis of stair ambulation in lower limb amputees, Gait & Posture, 2007, 25(2), pp. 267–278, https://doi.org/10.1016/j.gaitpost.2006.04.008

[9] S. M. Jaegers, J. H. Arendzen, and H. J. de Jongh, "Prosthetic gait of unilateral transfemoral amputees: A kinematic study," Arch. Phys. Med. Rehabil., vol. 76, no. 8, pp. 736–743, 1995.

[10] S. Mochon and T. A. McMahon, 'Ballistic walking', J Biomech, vol. 13, no. 1, pp. 49–57, 1980, doi: 10.1016/0021-9290(80)90007-x.

[11] S. Mochon and T. A. McMahon, 'Ballistic walking: an improved model', Mathematical Biosciences, vol. 52, no. 3, pp. 241–260, Dec. 1980, doi: 10.1016/0025-5564(80)90070-X.

[12] D. W. W. Heitzmann, J. Block, T. Kaib, S. I. Wolf, and M. Alimusaj, 'O 013– compensatory mechanisms in people with a trans-femoral amputation to guarantee adequate toe clearance of the prosthetic limb during stair climbing', Gait & Posture, vol. 65, pp. 23–24, Sep. 2018, doi: 10.1016/j.gaitpost.2018.06.031.

[13] C. Fanciullacci et al., 'Survey of transfemoral amputee experience and priorities for the user-centered design of powered robotic transfemoral prostheses', Journal of NeuroEngineering and Rehabilitation, vol. 18, no. 1, p. 168, Dec. 2021, doi: 10.1186/s12984-021-00944-x.

[14] A. T. Sugawara, V. D. Ramos, F. M. Alfieri, and L. R. Battistella, 'Abandonment of assistive products: assessing abandonment levels and factors that impact on it', Disabil Rehabil Assist Technol, vol. 13, no. 7, pp. 716–723, Oct. 2018, doi: 10.1080/17483107.2018.1425748.

[15] A. F. Azocar, L. M. Mooney, J.-F. Duval, A. M. Simon, L. J. Hargrove, and E. J. Rouse, 'Design and clinical implementation of an open-source bionic leg', Nat Biomed Eng, vol. 4, no. 10, Art. no. 10, Oct. 2020, doi: 10.1038/s41551-020-00619-3.

[16] T. Elery, S. Rezazadeh, C. Nesler, and R. D. Gregg, 'Design and Validation of a Powered Knee–Ankle Prosthesis With High-Torque, Low-Impedance Actuators', IEEE Trans. Robot., vol. 36, no. 6, pp. 1649–1668, Dec. 2020, doi: 10.1109/TRO.2020.3005533.

[17] S. Pheasant, Bodyspace: Anthropometry, Ergonomics And The Design Of Work: Anthropometry, Ergonomics And The Design Of Work, 2nd ed. London: CRC Press, 2014. doi: 10.1201/9781482272420.

[18] Ottobock. Ottobock C-Leg Prosthetic Product Page. [Online]. Available: https://www.ottobock.com/it-it/product/3C88-3 23C98-3

[19] R. Riener, M. Rabuffetti, and C. Frigo, 'Stair ascent and descent at different inclinations', Gait & Posture, vol. 15, no. 1, pp. 32–44, Feb. 2002, doi: 10.1016/S0966-6362(01)00162-X.

[20] E. Perreault, L. Hargrove, D. Ludvig, H. Lee, and J. Sensinger, 'Considering Limb Impedance in the Design and Control of Prosthetic Devices', in Neuro-Robotics: From Brain Machine Interfaces to Rehabilitation Robotics, P. Artemiadis, Ed., in Trends in Augmentation of Human Performance. , Dordrecht: Springer Netherlands, 2014, pp. 59–83. doi: 10.1007/978-94-017-8932-5_3.

[21] E. C. Honert and K. E. Zelik, 'Foot and shoe responsible for majority of soft tissue work in early stance of walking', Human Movement Science, vol. 64, pp. 191–202, Apr. 2019, doi: 10.1016/j.humov.2019.01.008.

[22] D. A. Winter, Biomechanics and motor control of human movement, 4th ed. Hoboken, N.J: Wiley, 2009.

[23] H. van der Kooij et al., 'Identification of Hip and Knee Joint Impedance During the Swing Phase of Walking', IEEE Trans Neural Syst Rehabil Eng, vol. 30, pp. 1203–1212, 2022, doi: 10.1109/TNSRE.2022.3172497.

[24] S. C. Culver, L. G. Vailati, and M. Goldfarb, 'A Power-Capable Knee Prosthesis With Ballistic Swing-Phase', IEEE Transactions on Medical Robotics and Bionics, vol. 4, no. 4, pp. 1034–1045, Nov. 2022, doi: 10.1109/TMRB.2022.3216475.

[25] M. Tran, L. Gabert, S. Hood, and T. Lenzi, 'A lightweight robotic leg prosthesis replicating the biomechanics of the knee, ankle, and toe joint', Science Robotics, vol. 7, no. 72, p. eabo3996, Nov. 2022, doi: 10.1126/scirobotics.abo3996.

[26] A. R. Tilley, H. Dreyfuss, and H. D. Associates, The Measure of Man and Woman: Human Factors in Design. Whitney Library of Design, 1993. [Online]. Available: https://books.google.it/books?id=5qzHQgAACAAJ

[27] U. H. Lee et al., 'How to Model Brushless Electric Motors for the Design of Lightweight Robotic Systems'. arXiv, Sep. 29, 2023. doi: 10.48550/arXiv.2310.00080.

[28] J.-Y. Li, Z.-H. Zhan, Y. Li, and J. Zhang, 'Multiple Tasks for Multiple Objectives: A New Multiobjective Optimization Method via Multitask Optimization', IEEE Trans. Evol. Computat., pp. 1–1, 2024, doi: 10.1109/TEVC.2023.3294307.

[29] J. Zhu, C. Jiao, I. Dominguez, S. Yu, and H. Su, 'Design and Backdrivability Modeling of a Portable High Torque Robotic Knee Prosthesis With Intrinsic Compliance for Agile Activities', IEEE/ASME Transactions on Mechatronics, vol. 27, no. 4, pp. 1837–1845, Aug. 2022, doi: 10.1109/TMECH.2022.3176255.

[30] T. Lencioni, I. Carpinella, M. Rabuffetti, A. Marzegan, and M. Ferrarin, 'Human kinematic, kinetic and EMG data during different walking and stair ascending and descending tasks', Sci Data, vol. 6, no. 1, p. 309, Dec. 2019, doi: 10.1038/s41597-019-0323-z.

[31] J. Camargo, A. Ramanathan, W. Flanagan, and A. Young, 'A comprehensive, open-source dataset of lower limb biomechanics in multiple conditions of stairs, ramps, and level-ground ambulation and transitions', Journal of Biomechanics, vol. 119, p. 110320, Apr. 2021, doi: 10.1016/j.jbiomech.2021.110320.